sensors

MDPI

Article

Emission Flux Measurement Error with a Mobile DOAS System and Application to NO_x Flux Observations

Fengcheng Wu [1], Ang Li [1,*], Pinhua Xie [1,2,3,*], Hao Chen [1], Zhaokun Hu [1], Qiong Zhang [1], Jianguo Liu [1] and Wenqing Liu [1]

1 Key Laboratory of Environmental Optical and Technology, Anhui Institute of Optics and Fine Mechanics, Chinese Academy of Sciences, Hefei 230031, China; fcwu@aiofm.ac.cn (F.W.); hchen@aiofm.ac.cn (H.C.); zkhu@aiofm.ac.cn (Z.H.); zhangqiong@aiofm.ac.cn (Q.Z.); jgliu@aiofm.ac.cn (J.L.); wqliu@aiofm.ac.cn (W.L.)

2 Center for Excellence in Regional Atmospheric Environment, Institute of Urban Environment, Chinese Academy of Sciences, Xiamen 361021, China

3 School of Environmental Science and Optoeclectronic Technology, University of Science and Technology of China, Hefei 230026, China

* Correspondence: angli@aiofm.ac.cn (A.L.); phxie@aiofm.ac.cn (P.X.); Tel.: +86-551-6559-3690 (A.L.); +86-551-6559-3147 (P.X.)

Academic Editor: Jason K. Levy
Received: 15 December 2016; Accepted: 19 January 2017; Published: 25 January 2017

Abstract: Mobile differential optical absorption spectroscopy (mobile DOAS) is an optical remote sensing method that can rapidly measure trace gas emission flux from air pollution sources (such as power plants, industrial areas, and cities) in real time. Generally, mobile DOAS is influenced by wind, drive velocity, and other factors, especially in the usage of wind field when the emission flux in a mobile DOAS system is observed. This paper presents a detailed error analysis and NOx emission with mobile DOAS system from a power plant in Shijiazhuang city, China. Comparison of the SO_2 emission flux from mobile DOAS observations with continuous emission monitoring system (CEMS) under different drive speeds and wind fields revealed that the optimal drive velocity is 30–40 km/h, and the wind field at plume height is selected when mobile DOAS observations are performed. In addition, the total errors of SO_2 and NO_2 emissions with mobile DOAS measurements are 32% and 30%, respectively, combined with the analysis of the uncertainties of column density, wind field, and drive velocity. Furthermore, the NO_x emission of 0.15 ± 0.06 kg/s from the power plant is estimated, which is in good agreement with that from CEMS observations of 0.17 ± 0.07 kg/s. This study has significantly contributed to the measurement of the mobile DOAS system on emission from air pollution sources, thus improving estimation accuracy.

Keywords: DOAS; spectrophotometer; mobile measurements; emission flux; error; NO_x

1. Introduction

China has been experiencing severe air pollution problem with the booming growth of industrialization and urbanization. The key to alleviate air pollution is the measurement, supervision, and control of its sources. The emission flux of sources is the most important and fundamental data for pollution source assessment. Currently, the primary technique for detecting emission flux is field test method, which calculates organized pollution emission based on observations of exhaust flow rate and air pollutant concentrations. However, the method cannot detect fugitive emissions, especially in area sources. In addition, the model [1,2] is also an alternative method for estimating source emission; however, it is limited to spatial scale and real-time data.

Mobile differential optical absorption spectroscopy (mobile DOAS) [3,4] is a novel optical remote method that can estimate source emission. The technique was developed from fixed-scanning DOAS [5] observation of volcanoes and measurement of point emissions (power plants, oil refineries, etc.) and area (city, industrial areas, etc.) sources with zenith-observation DOAS system mounted on a mobile platform. Johansson et al. [3,4] and Rivera et al. [6] estimated SO_2, NO_2, and HCHO emissions from the industrial areas in Mexico, Beijing, and Tula (Mexico) with mobile DOAS from 2008 to 2009. NOx emissions in Mannheim, Ludwigshafen, and New Delhi city were observed by Ibrahim et al. [7] and Shaiganfar et al. [8] in 2010 and 2011 with mobile multi-axis differential optical absorption spectroscopy (mobile MAX-DOAS). From these studies, mobile DOAS has provided a novel and rapid method for source emission measurement. However, one disadvantage of this method is that the observation is affected by actual conditions (such as weather, wind, etc.). Previous studies [6] suggesting either near-surface wind from a ground meteorological station or wind at plume height from a model can be used to estimate emission. However, a detailed discussion on errors from different wind and drive speeds with mobile DOAS observations still lacks. In the current study, one power plant in Shijiazhuang city is selected as a typical point source to discuss the usage of the appropriate wind and drive speed for emission measurement using mobile DOAS. Furthermore, the total emission error of mobile DOAS is estimated based on error analysis for each impact factor of emission measurement.

Meanwhile, as one significant application of mobile DOAS, the NO_x emission from a power plant is estimated. NO_x is one of the most important trace gases in the atmosphere [9]. It participates in the catalytic formation of ozone (O_3) in the troposphere, while being a catalyst for O_3 destruction in the stratosphere [10,11]. NO_x sources include nature source and anthropogenic source. The main anthropogenic sources are fossil fuels (coal, oil, etc.) and biomass burning. This study explores the observation of NO_x emission from power plants with mobile DOAS preliminary and compares it with the CEMS result, showing a good agreement between the two results.

2. Experiment and Principles

2.1. Overview of Experiment

A power plant with stack height of 180 m was located at the south of Shijiazhuang city, a typical point source surrounded by farmlands. The construction of the power plant was divided into two stages: The first stage involves the construction of two coal-fired heating units with a total power of 600 MW, which are currently in operation. The second stage plans the construction of another two coal-fired heating units with total power of 700 MW, which is currently being actively promoted. The measurements were conducted from October to November 2011. The entire weather condition was dominated by clouds, and rain occasionally poured from 3 November to 5 November and from 7 November to 8 November for each measurement day, we conducted circular measurements and performed scanning measurements in the north of the power plant, considering good driving conditions for different drive speeds. The entire circle and scanning route was 12 km and 6 km, respectively. We took approximately 30 and 15 min to complete the measurements. The measurement time was from 10:00 to 14:30. Furthermore, one wind LIDAR, MAX-DOAS, and some point instruments detected NO, NO_2, and O_3 concentrations established away from the power plant (1.7 km). The setup of the measurement sites and two different driving routes are shown in Figure 1.

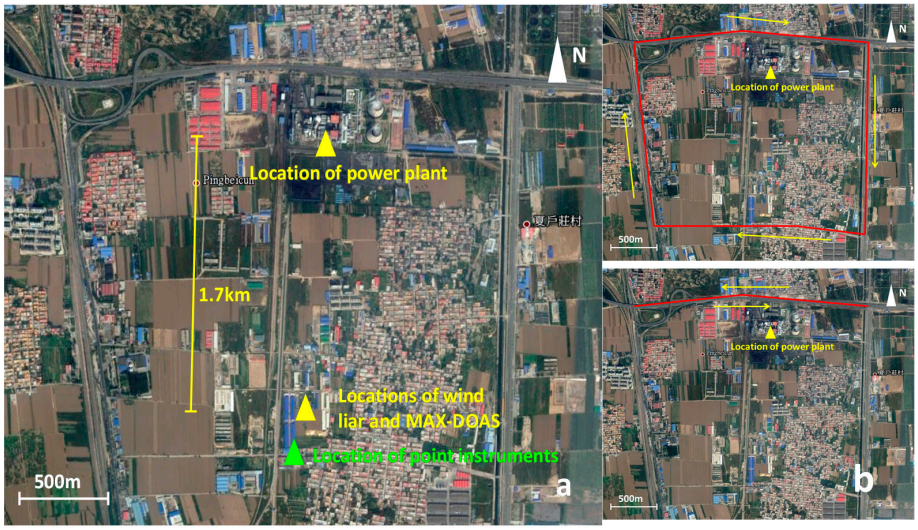

Figure 1. Setup of measurement sites (**a**) and two different driving routes (**b**). Red lines indicate the measurement routes and yellow arrows indicate the driving direction in the (**b**).

2.2. Mobile DOAS System

The mobile DOAS system was developed at the Anhui Institute of Optics and Fine Mechanics as shown in Figure 2 [12]. The components of the instrument are spectra acquiring unit, data processing unit, and global position system (GPS) module. The spectra acquiring unit includes a zenith observation telescope and optics miniature spectrometer. The telescope collects scattered sunlight in the zenith observation and focuses into a fiber. Light collected by the telescope is transmitted to the spectrometer (HR2000+, Ocean Optics, Dunedin, FL, USA) through the fiber with spectral resolution of 0.6 nm and spectral wavelength range of 290–420 nm. The spectra are then transmitted to the data processing unit to retrieve the concentration in real time through a USB data cable. GPS module is used to record geographic information and drive speed information. The system is also equipped with a miniature weather station mounted on top of the measurement van to obtain meteorological data (wind direction, wind speed, temperature, pressure, etc.). Details of the instrument and its performance are described in our previous study [13].

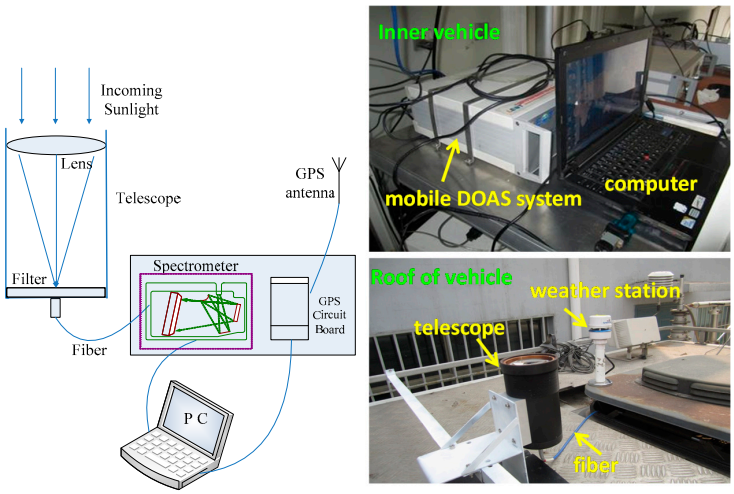

Figure 2. Mobile DOAS system.

2.3. Principle of Mobile DOAS

2.3.1. Retrieval of Vertical Column Density

The passive DOAS technique has been employed in numerous applications that use sunlight with instruments mounted on various fixed or mobile platforms [14–19]. The evaluation procedure is described in this section in relation to our mobile observation. Details of DOAS analysis are presented in Platt and Stutz (2008) [20].

The zenith scattered sunlight I_0 is collected by the mobile DOAS as I due to atmospheric extinction. I and I_0 agree with the Lambert-Beer law:

$$I = I_0 \cdot \exp(-\sigma \cdot c \cdot L) \tag{1}$$

where σ (unit: cm^2/molec.) is the cross section of trace gas, c (unit: molec./cm^3) is the concentration, and L (unit: cm) is the length of the absorption route. The concentration of trace gas can be evaluated based on the least square fit algorithm using Equation (1). Unknown to the length of absorption route with mobile DOAS observations, the slant column density (SCD, unit: molec./cm^2) can be retrieved using Equation (1). The SCD is defined as the trace gas concentration integrated along the effective light path:

$$SCD = \int c(l) \cdot dl = \frac{1}{\sigma}(\frac{I_0}{I}) \tag{2}$$

The vertical column density (VCD) (unit: molecules/cm^2) can be calculated with the SCD and air mass factor (AMF, non-dimensional variable) [21] as shown in Equation (3). The AMF can be obtained with radiation transfer model and geometric approximation, which depends on the solar zenith angle, wavelength, and elevation angle:

$$VCD = \frac{SCD}{AMF} \tag{3}$$

2.3.2. Estimation of Emission

The emission of source can be detected in combination with the VCD and the measurement route, wind speed, and wind direction. For one area of interest, the emission flux is calculated using Equation (4) [3,4,7]:

$$F = \int_A div(VCD \cdot \vec{W}) \cdot dA = \oint_S VCD(\vec{s}) \cdot \vec{W} \cdot \vec{n} \cdot d\vec{s} \tag{4}$$

where $\vec{W}$ indicates the average wind vector, A indicates the encircled area, $\vec{n}$ indicates the normal vector parallel to the Earth's surface and orthogonal to the driving direction at the position of the driving route, and $\vec{s}$ is the driving route. For mobile DOAS measurements, we can convert Equation (4) to Equation (5):

$$F = \sum_i VCD(s_i) \cdot \vec{W} \cdot \vec{n} \cdot \Delta s_i = \sum_i VCD(s_i) \cdot \vec{W} \cdot \sin(\beta)(s_i) \cdot \Delta s_i \tag{5}$$

where β is the angle between the driving direction and wind direction, and Δs_i is the distance between two successive spectra.

The NOx emission is estimated based on the conversion of NO_2 emission with two correction factors: chemical transformation factor and lifetime correction factor:

$$F_{NOx} = R \cdot c_L \cdot F_{NO_2} = R \cdot c_L \cdot \sum_i VCD_{NO_2}(s_i) \cdot \vec{W} \cdot \sin(\beta)(s_i) \cdot \Delta s_i \tag{6}$$

The chemical transformation factor can be written as R = NO_x/NO_2, NO_x = NO + NO_2:

$$R = \frac{NOx}{NO_2} = \frac{NO + NO_2}{NO_2} = 1 + \frac{NO}{NO_2} = 1 + c_\tau \quad (7)$$

$c_\tau = NO/NO_2$ is the Leighton ratio [11], which is generally derived from model simulations. In this study, we calculate the value from observation data of point instruments near the power plant.

c_L in Equation (6) is the lifetime correction factor, which is derived using Equation (8):

$$c_L = e^{\frac{D/W}{t}} \quad (8)$$

where D (unit: meters) is the mean distance from the source to the measurement site of about 2 km during this observation. t (unit: second) indicates the NOx lifetime, which depends on photochemical reaction and meteorological condition and is difficult to determine for the specific situation of our measurements. We use an average value of 5 h for the NOx lifetime, which is derived from long-term satellite observations of polluted area in summer and autumn in eastern China [22].

2.4. Data Analysis

The VCDs of SO_2 and NO_2 are retrieved through the DOAS method as discussed in Section 2.3.1. During our retrieval process, a spectrum is first selected arbitrarily on the upwind path as reference spectrum to determine the concentration distribution trends along the route. The minimum concentration of SO_2 and NO_2 along each driving route is then chosen as the Fraunhofer spectra to re-retrieve the measurement spectra.

The wavelength range of 310 to 324 nm with three strong absorption peaks is selected for the SO_2 fit. Absorption cross sections of SO_2, NO_2, HCHO, O_3 (Bogumil et al. [23]), and Ring are included in the fit. The Ring spectrum is generated from the measured Fraunhofer reference spectrum using the DOASIS [24] software. For the analysis of NO_2, the wavelength range of 345 to 365 nm is selected, and the cross section of O_4 at 298 K is also included, except for NO_2, HCHO, O_3 at 293 K (Bogumil et al. [23]), and Ring spectrum. The wavelength calibration is performed using a highly resolved solar spectrum (Kurucz et al. [25]) convoluted by the instrument's slit function. The software of WinDOAS [26] is used to evaluate the SO_2 and NO_2 SCDs. An example for such a spectral fitting is shown in Figure 3, where the SCD is 1.92 × 10^{17} ± 6.56 × 10^{15} molec./cm^2 and 5.76 × 10^{16} ± 1.53 × 10^{15} molec./cm^2 for SO_2 and NO_2, respectively. The fit uncertainties of retrieved values from these two spectra for SO_2 and NO_2 are about 3.41% and 2.66%, respectively. For all measured spectra, the fit uncertainties are less than 15% for NO_2 and 20% for SO_2.

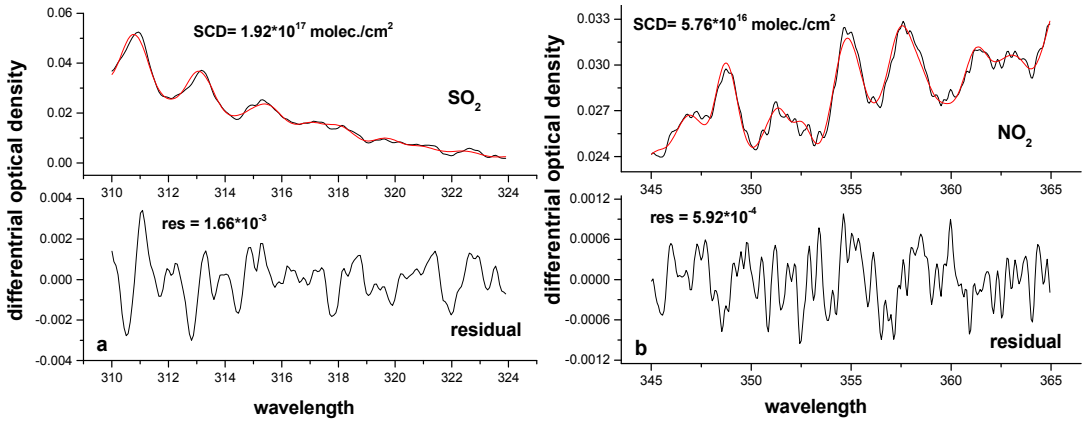

Figure 3. SO_2 and NO_2 fitting. The spectra are recorded at the time of 12:35:02 on 16 October 2011. (**a**) SO_2 retrieval result, SO_2 SCD = 1.92 × 10^{17} molec./cm^2, SO_2 residual = 1.66 × 10^{-3}; (**b**) NO_2 retrieval result, NO_2 SCD = 5.76 × 10^{16} molec./cm^2, NO_2 residual = 5.92 × 10^{-4}.

In the previous study, the VCDs of SO_2 and NO_2 were derived through the geometric approximation of AMF with mobile DOAS observation. According to the relationship between AMF and elevation angle ($AMF_{trop} \approx 1/\sin(\alpha)$), the tropospheric AMF is close to 1 due to zenith observation and measurement time at noon. As a result, the retrieved SCD is approximated to VCD. However, AMF_{NO2} is larger than 1 (Figure 4a,b) and AMF_{SO2} is approximately equal to 1 (Figure 4c,d), which are retrieved using a radiative transfer model McArtim [27] simulation during the measurement time. In this study, the SO_2 and NO_2 VCDs are calculated using the simulated AMF.

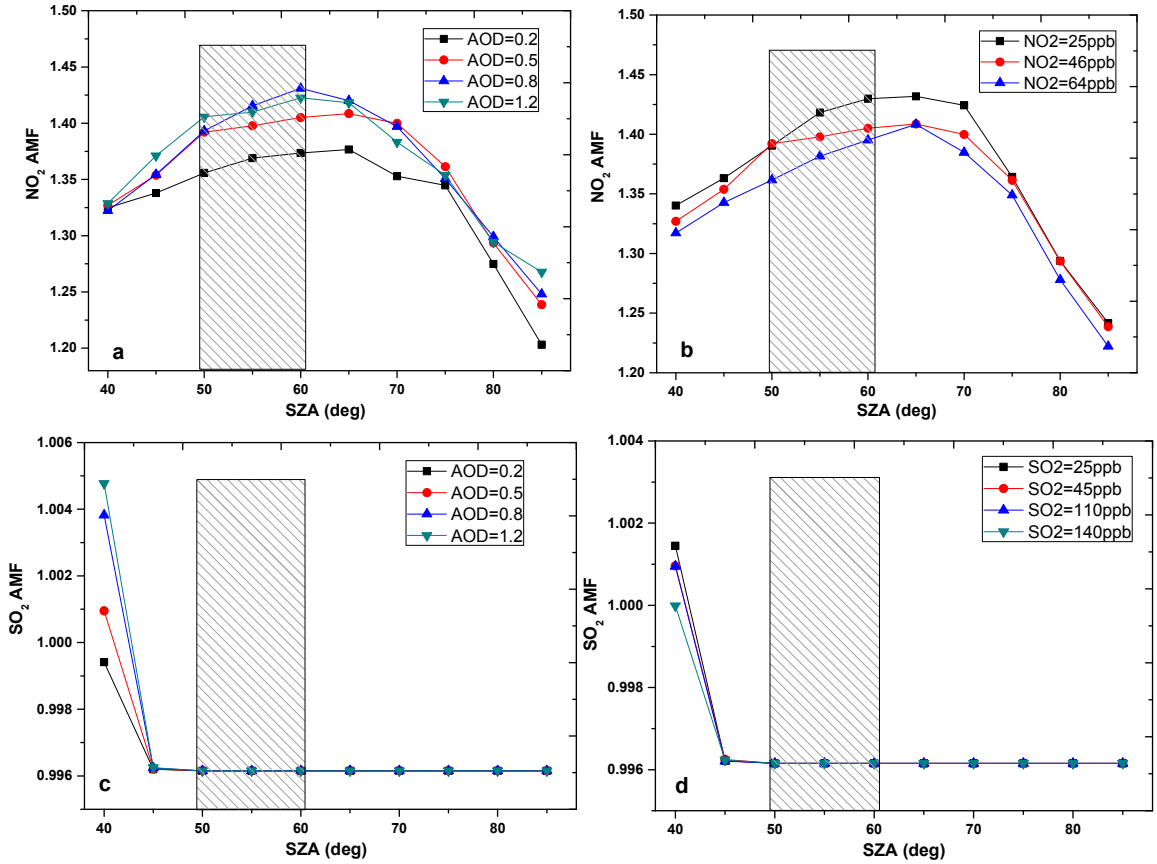

Figure 4. Simulated AMF for different aerosol and trace gas profiles. The rectangle regarding the solar zenith angle (SZA) is the time of mobile DOAS observations. (**a**) NO_2 AMF simulation in the scenarios of different SZAs and aerosol optical density (0.2, 0.5, 0.8 and 1.2); (**b**) NO_2 AMF simulation in the scenarios of different SZAs and NO_2 concentration (25 ppb, 46 ppb and 64 ppb) (**c**) SO_2 AMF simulation in the scenarios of different SZAs and aerosol optical density (0.2, 0.5, 0.8 and 1.2); (**d**) SO_2 AMF simulation in the scenarios of different SZAs and SO_2 concentration (25ppb, 45 ppb, 110 ppb and 140 ppb).

AMF strongly depends on NO_2 and aerosol profiles, which use radiative transfer model simulation. The different scenarios of aerosol, SO_2, and NO_2 are set to estimate the uncertainties of SO_2 and NO_2 AMF (Figure 4). The height of boundary layer is taken from LIDAR and ceilometer observations away from mobile DOAS (5 km). The concentrations of SO_2 and NO_2 are taken from point instruments near the power plant. The average boundary layer is about 1 km, and aerosol optical density (AOD) ranged from 0.2 to 1.2 as observed from the LIDAR and ceilometer. We assumed that the aerosol profiles are given by constant values below the boundary layer height and exponential profiles above for the AMF simulation. The NO_2 scenarios of 64, 25, and 46 ppb and SO_2 scenarios of 25, 45, 110, and 140 ppb are set based on the data from point instruments. The NO_2 and SO_2 profiles are given with a "box" shape, only aiming at plume observation from the power plant.

NO_2 AMF uncertainties are about 6%, caused by aerosol and NO_2 profiles during the measurement period (the solar zenith angle between 50° and 60°) from Figure 4. However, the SO_2 AMF is free of solar zenith angle, aerosol, and SO_2 variations. As a result, the uncertainties of SO_2 AMF can be neglected compared with other errors.

3. Analysis of Mobile DOAS Error

3.1. Usage of Driving Speed

The selection of driving speed is a key factor for mobile DOAS observations, and the peak value may be lost if the driving speed is too fast. Otherwise, the conversion may be yielded for emission plume resulting in inconsistency between emission and measurement if the speed is too low. Thus, the selection of appropriate speed represented by sampling points during plume observation is important to accurately estimate emission. We have estimated the SO_2 emission for different samples and compared them with those of CEMS. The optimal sampling is achieved by intercomparison of CEMS and mobile DOAS, and the optimal speed is presented combined with plume width and sampling time.

The average width of plume is calculated based on multiple scanning measurements for different sampling assuming similar weather conditions:

$$L = \frac{\sum_{i=1}^{n} v_i \cdot s_i \cdot \Delta t_i}{n} \tag{9}$$

where n indicates the number of times of all scanning measurements, v_i is the driving speed for each scanning measurement, and s_i indicates the number of sampling for each scanning measurement. The average plume width, optimal sampling, and optimal speed are shown in Figure 5. The maximum and minimum plume width is 1.28 ± 0.07 km and 0.53 ± 0.11 km, respectively, during the measurement period. The intercomparison of the results between CEMS and mobile DOAS and the sampling with the minimum difference, which is the optimal sampling, are shown in Figure 5. The optimal driving speed of 36.21 ± 5.44 km/h is calculated based on the average plume width, optimal sampling, and sampling time.

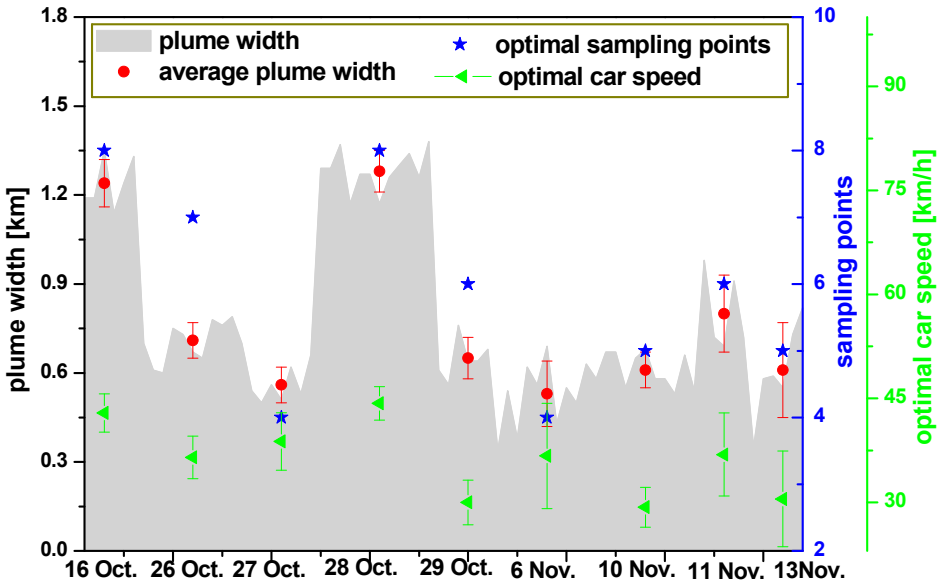

Figure 5. Plume width, average plume width, optimal sampling, and speed.

3.2. Usage of Wind

Wind information is one of the largest error sources in emission estimation. The question on the usage of ground-based wind or plume-height wind has not been discussed in detail in previous studies. As shown in Figure 1, one wind LIDAR is set up near the power plant to obtain the vertical wind data, particularly the wind data at 200 m height. Meanwhile, we also access this data from MM5 model [28] simulation except for the LIDAR. The ground-based wind data (the altitude is about 10 m) are taken from the miniature weather station mounted on the car.

The SO_2 emission is estimated with ground-based wind and plume-height wind for different sampling as discussed in Section 3.1 and compared with CEMS results. Figure 6 demonstrates two examples of SO_2 emission on 26 October and 10 November under different conditions.

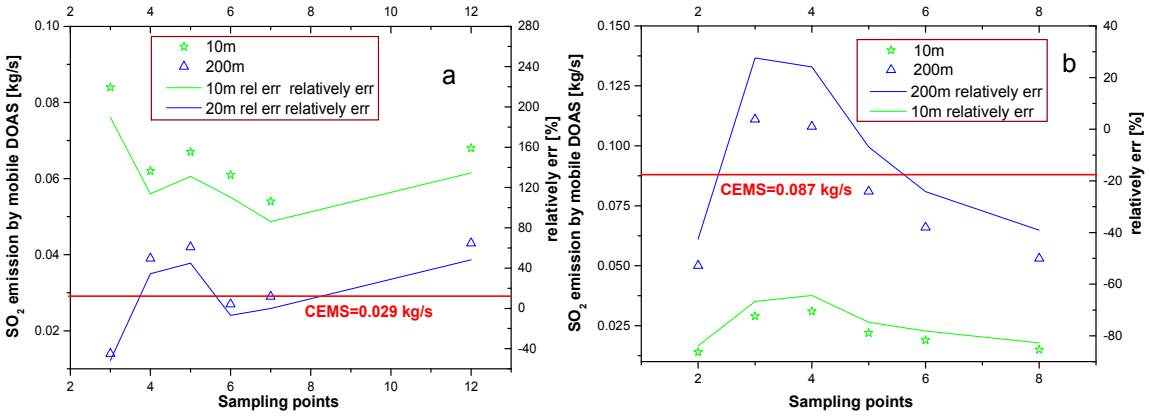

Figure 6. SO_2 emission and relative deviation. (**a**) SO_2 emission results on 26 October; (**b**) SO_2 emission results on 10 November. The dots and lines indicate SO_2 emission and relative deviation, respectively. The negative relative deviation indicates that the mobile DOAS result is lower than that of CEMS.

The emission result is closer to that of CEMS when it calculates the emission with 200 m height wind. In this case, the 200 m height is the source from the stack height of 180 m. In addition, further results suggest the difference between mobile DOAS and CEMS, which is lower when the 200 m height wind and driving speed of 30–40 km/h are used to calculate emission.

3.3. Comparison of SO_2 Emission Using Different Wind Data

As discussed in Section 3.2, the SO_2 emission estimation using mobile DOAS is more accurate when the plume height wind is adopted. The plume height wind is mainly sourced from sounding balloon, model simulation, and wind LIDAR. However, these data rather than ground-based wind data for actual measurement in general are difficult to access. To evaluate the SO_2 emission error caused by wind, the ground-based wind, 200 m height wind from wind LIDAR or model, and 200 m height wind calculation from ground-based wind are used to estimate emission, and the detailed error analysis for the three types of wind data are performed in this study.

The empirical formula [29] of wind profile shows that the relationship of ground-based wind speed and different altitudes of wind speed, with altitude $z \leq 200$ m, is as follows:

$$u = u_0 \cdot \left(\frac{z}{z_0}\right)^m \tag{10}$$

where z_0 is the altitude of the ground-based weather station (z_0 = 10 m), u_0 is the wind speed at the altitude of z_0, and m is a factor that relates to atmospheric stability with m = 0.15 [29] for "D-class" and m = 0.10 for "C-class". This "C- or D-class" sources from six Pasquill–Turner stability class are derived from the combination of wind speed, solar radiation, and cloud cover: from 1 or A for extremely

unstable to 6 or F for extremely stable conditions [30,31]. The atmospheric stability of "D-class" is selected for the majority of measurement time (16, 27 and 29 October and 6, 10, 11 and 13 November), except for 26 October and 28 October, which are regarded as "C-class." The related classifications are discussed in our previous study, which takes into account wind speed, solar radiation, and cloud cover [28].

Figure 7 shows the ground-based wind speed (referred to as A1), 200 m height wind speed source from wind LIDAR or model (referred to as B1), and 200 m height wind speed with calculation from ground-based wind (referred to as C1). The wind speed of A1 is lower than those of B1 and C1. Apart from the wind speed on 10 November and 13 November with the largest difference of 1.06 m/s and 0.86 m/s, respectively, C1 agrees with B1 in most of the conditions. In addition, the wind speed trend is in good agreement for A1, B1, and C1, except for 29 October and 10 November.

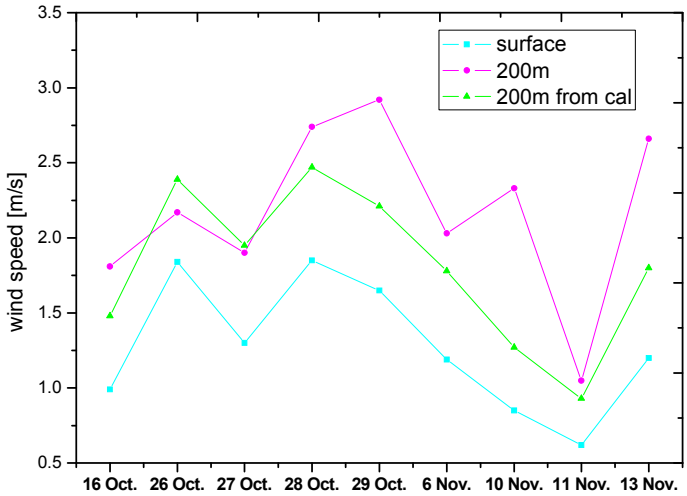

Figure 7. Three types of wind speed. Blue indicates the wind speed source from ground-based wind; pink indicates the wind speed source from 200 m height (LIDAR or model); and green indicates the wind speed source from 200 m height with calculation from ground-based wind.

Figure 8 shows that the SO_2 emission estimations with B1 and C1 winds are larger than those with A1 as presented in Figure 6 in majority of the cases. However, the SO_2 emission with A1 wind is larger than those with B1 and C1 on 26 October and 28 October because of the deviation of wind direction between ground-based wind and 200 m altitude. The ratios of emission estimation with C1 and B1 winds fluctuate around 1, whereas the maximum ratio is 1.81 and 1.88 on 26 October and 28 October, respectively. This scenario can be explained by the fact that we also consider the wind direction more than wind speed when estimating the emission. However, the empirical formula as presented in Equation (10) reveals that the wind speed at an altitude of 200 m and the hypothesis of wind direction for C1 and A1 agree are prerequisites when calculating the emission with C1 wind. In other words, the significant difference of wind direction between B1 wind and C1 wind can result in large deviation in emission estimation using B1 and C1 winds.

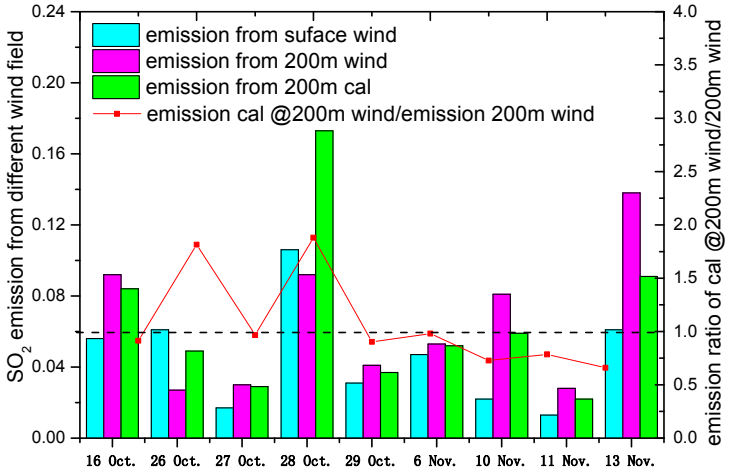

Figure 8. SO_2 emission estimation with different types of wind and ratios of emission with C1 and B1 wind.

Table 1 lists the SO_2 emission from mobile DOAS observations with three different wind and CEMS observations. It shows that the similar trends of relative deviation between CEMS and SO_2 estimation with B1 and C1 winds based on mobile DOAS are presented apart from the results of 26 October and 28 October.

Table 1. Comparison of SO_2 emission between mobile DOAS for three different winds and CEMS. The percentage indicates the deviation with respect to emission from CEMS. The negative values imply that CEMS is lower than those from mobile DOAS; the positive values imply otherwise.

	Emission from CEMS kg/s	Surface Wind %	200 m Wind %	Calculation at 200 m Wind %
16 October	0.096	−41.67	−4.17	−12.50
26 October	0.029	110.34	−6.90	68.97
27 October	0.042	−59.52	−28.57	−30.95
28 October	0.069	53.62	33.33	150.72
29 October	0.139	−77.70	−70.50	−73.38
6 November	0.064	−26.56	−17.19	−18.75
10 November	0.087	−74.71	−6.90	−32.18
11 November	0.056	−76.79	−50.00	−60.71
13 November	0.119	−48.74	−15.97	−23.53

However, although the emission estimation with B1 and C1 winds has a small difference, their ratio fluctuates around 1, which can be explained by the errors of empirical formula and the value of m. In addition, the relatively low deviations for emission estimation with the wind of 200 m height further verify the discussions in Section 3.1. The result of the relatively larger deviations is caused by the fog weather on 29 October. If the plume height wind is difficult to access, then we could estimate emission with the wind calculation from ground-based wind using the empirical formula based on the mobile DOAS observations when the weather system is relatively stable and when vertical wind direction has no significant variation.

3.4. Total Errors of Emission Flux

According to the above analysis, the relative deviations of emission estimation are lower under a drive velocity of 30–40 km/h, and the wind field at plume height is selected when flux is calculated. However, the total errors of mobile DOAS have not been listed. This section discusses the total errors

of emission flux based on the mobile DOAS observations. The total errors of emission flux can be calculated using Equation (11):

$$\frac{\Delta F_i}{F_i} = \sqrt{\left(\frac{\Delta \vec{W}}{\vec{W}}\right)^2 + \left(\frac{\Delta SCD}{SCD}\right)^2 + \left(\frac{\Delta AMF}{AMF}\right)^2 + \left(\frac{\Delta s}{s}\right)^2} \quad (11)$$

From the above formula, four components are included in emission estimation errors: wind error ($\Delta\vec{W}$), SCD (ΔSCD) error, AMF (ΔAMF) error, and distance difference (Δs, represented by drive velocity) error. The accuracy of drive speed is about 1% resulting from GPS. The drive speed variation is 1 km/h, and the flux can change by 2% to 3% from the actual calculation. Thus, the variation of 0.3–0.4 km/h (the optimal speed is 30–40 km/h) for drive velocity can result in a change in approximately 1% on emission estimation. As a result, the distance difference error is 1%. In addition, the SCD errors of SO_2 and NO_2 are low at 20% and 15%, respectively, and the AMF error of NO_2 is about 6%. According to the discussions in Section 2.4, the AMF error of SO_2 is negligible during the measurement periods. Furthermore, the largest error source of emission estimation is from wind field, including wind direction and wind speed errors as listed in Table 2. The average wind error is about 25%, considering the uncertainties of wind direction and wind speed. As a result, the total estimation errors of SO_2 and NO_2 are 32% and 30%, respectively.

Table 2. Wind field uncertainty of emission estimation.

Date	Time	Wind Direction (Degree)	Wind Speed (m/s)	Uncertainties from Wind Direction	Uncertainties from Wind Speed	Uncertainties from Wind
16 October	10:00–12:00	274.13 ± 2.15	1.81 ± 0.4	1%	22%	22%
26 October	12:30–14:00	135.25 ± 9.51	2.17 ± 0.2	14%	10%	17%
27 October	12:00–13:00	123 ± 6	1.9 ± 0.3	19%	14%	24%
28 October	11:40–13:00	183.02 ± 10.10	2.74 ± 0.42	2%	15%	16%
29 October	13:30–14:10	112.21 ± 1.81	2.92 ± 0.36	10%	12%	16%
6 November	11:00–13:00	230.8 ± 12	2.03 ± 0.64	24%	33%	41%
10 November	13:00–14:30	167.67 ± 9.46	2.33 ± 0.54	3%	24%	25%
11 November	11:30–12:10	211.17 ± 28.06	1.05 ± 0.29	33%	29%	44%
13 November	11:40–12:10	192.58 ± 7.29	2.66 ± 0.61	3%	23%	24%

3.5. Emission Estimation of NOx

From Equation (6), the prerequisite for estimation of NOx emission is the knowledge of the ratio of NO and NO_2, which is expected to be established for ozone-rich condition. However, the measurements are performed close to the stacks of power plants. The reaction of NO with ozone will eventually consume all available ozone, which prevents further conversion of NO into NO_2. Only after additional ozone-rich air is mixed with the ozone-depleted air masses can the ratio be established. Thus, we analyze the NO, NO_2, and O_3 concentration from point instrument observations located 1.7 km away from the power plant during the measurement period of this study. We calculate the ratio of NO and NO_2 (Table 3) under an O_3 concentration higher than NO concentration. Moreover, the NO_x lifetime factor is calculated using wind speed with Equation (8).

Table 3. NO, NO_2, and O_3 concentration and the values of R and C_L.

Date	NO mg/m^3	NO_2 mg/m^3	Leighton Ratio	O_3 mg/m^3	R	C_L	Wind Speed m/s
16 October	0.041	0.072	0.57	0.042	1.57	1.06	1.81
19 October	0.014	0.041	0.34	0.024	1.34	1.04	3.00
28 October	0.04	0.116	0.34	0.048	1.34	1.06	2.74
6 November	0.015	0.044	0.34	0.048	1.34	1.07	2.03
10 November	0.028	0.063	0.44	0.028	1.44	1.05	2.33

The NOx emission is then estimated with R, C_L, and NO_2 emission flux (from mobile DOAS observation) based on Equation (6). Figure 9 shows the comparison of NO_x emission between mobile DOAS and CEMS, indicating a good agreement with the average flux of 0.15 ± 0.06 kg/s and 0.17 ± 0.07 kg/s from mobile DOAS and CEMS observations, respectively.

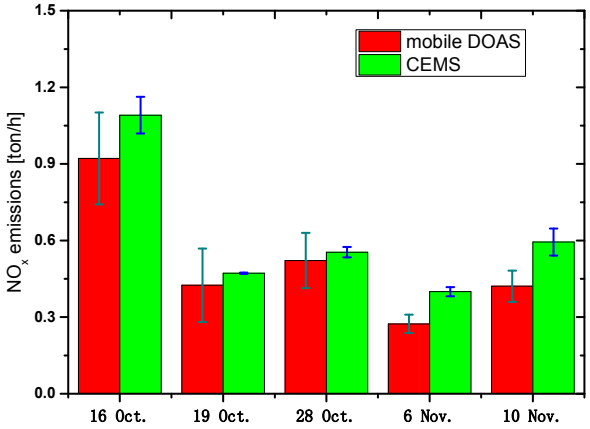

Figure 9. NO_X emission flux from mobile DOAS and CEMS observations.

4. Conclusions

A power plant in Shijiazhuang city was selected as the experimental site to study the emission flux estimation error with a mobile DOAS system under different measurement conditions and is explored to detect NO_x flux from power plant emission. This study has significantly contributed to the measurement of mobile DOAS on emission from air pollution sources, thus improving estimation accuracy.

The optimal drive velocity of 30–40 km/h and the wind field at plume height are selected when mobile DOAS observations are made by comparing the SO_2 emission flux from mobile DOAS with CEMS under different drive speeds and wind fields (ground-based and plume-height wind field). The emission flux can also be estimated with the plume-height wind speed based on empirical formula calculation when the weather system is relatively stable and vertical wind direction has no significant variation. In addition, the total error of mobile DOAS observations is estimated, which are sourced from wind field error, VCD error, and drive speed variation error. As a result, the total errors of SO_2 and NO_2 are 32% and 30%, respectively, taking into account wind field uncertainty of 25%, SO_2 SCD uncertainty of 20%, NO_2 SCD uncertainty of 15%, NO_2 AMF uncertainty of 6%, and drive speed uncertainty of 1%. Finally, the NOx emission from the power plant is estimated with a value of 0.15 ± 0.06 kg/s, which is in good agreement with that from CEMS observation with a value of 0.17 ± 0.07 kg/s.

Acknowledgments: This work was made possible by the support of the National Natural Science Foundation of China (41605013, 41275038, and 41530644) and Anhui Province Natural Science Foundation of China (1508085QD71).

Author Contributions: Pinhua Xie, Jianguo Liu and Wenqing Liu conceived, designed the experiments; Fengcheng Wu, Ang Li and Hao Chen performed the experiments; Fengcheng Wu, Zhaokun Hu and Qiong Zhang analyzed the data; Fengcheng Wu wrote the paper; Pinhua Xie and Ang Li improved the paper.

Conflicts of Interest: The authors declare no conflict of interest.

References

1. Lei, W.; de Foy, B.; Zavala, M.; Volkamer, R.; Molina, L.T. Characterizing Ozone Production in the Mexico City Metropolitan Area: A Case Study Using A Chemical Transport Model. *Atmos. Chem. Phys.* **2007**, *7*, 1347–1366. [CrossRef]
2. Zheng, J.Y.; Zhang, L.J.; Che, W.W.; Zheng, Z.Y.; Yin, S.S. A highly resolved temporal and spatial air pollutant emission inventory for the Pearl River Delta region, China and its uncertainty assessment. *Atmos. Environ.* **2009**, *43*, 5112–5122. [CrossRef]
3. Johansson, M.; Galle, B.; Yu, T.; Tang, L.; Chen, D.L.; Li, H.J.; Li, J.X.; Zhang, Y. Quantification of total emission of air pollutants from Beijing using mobile mini-DOAS. *Atmos. Environ.* **2008**, *42*, 6926–6933. [CrossRef]
4. Johansson, M.; Rivera, C.; de Foy, B.; Lei, W.; Song, J.; Zhang, Y.; Galle, B.; Molina, L. Mobile mini-DOAS measurement of the outflow of NO_2 and HCHO from Mexico City. *Atmos. Chem. Phys.* **2009**, *9*, 5647–5653. [CrossRef]
5. Galle, B.; Oppenheimer, C.; Geyer, A.; McGonigle, A.J.S.; Edmonds, M.; Horrocks, L. A miniaturised ultraviolet spectrometer for remote sensing of SO_2 fluxes: A new tool for volcano surveillance. *J. Volcanol. Geother. Res.* **2003**, *119*, 241–254. [CrossRef]
6. Rivera, C.; Sosa, G.; Wohrnschimmel, H.; De Foy, B.; Johansson, M.; Galle, B. Tula industrial complex (Mexico) emissions of SO_2 and NO_2 during the MCMA 2006 field campaign using a mobile mini-DOAS system. *Atmos. Chem. Phys.* **2009**, *9*, 6351–6361. [CrossRef]
7. Ibrahim, O.; Shaiganfar, R.; Sinreich, R.; Stein, T.; Platt, U.; Wagner, T. Car MAX-DOAS measurements around entire cities: Quantification of NOx emissions from the cities of Mannheim and Ludwigshafen (Germany). *Atmos. Meas. Tech.* **2010**, *3*, 709–721. [CrossRef]
8. Shaiganfar, R.; Beirle, S.; Sharma, M.; Chauhan, A.; Singh, R.P.; Wagner, T. Estimation of NOx emissions from Delhi using Car MAX-DOAS observations and comparison with OMI satellite data. *Atmos. Chem. Phys.* **2011**, *11*, 10871–10887. [CrossRef]
9. Elsayed, N.M. Toxicity of nitrogen dioxide: An introduction. *Toxicology* **1994**, *89*, 161–174. [CrossRef]
10. Jacob, D.J. *Introduction to Atmospheric Chemistry*; Princeton University Press: Princeton, NJ, USA, 1999.
11. Seinfeld, J.H.; Pandis, S.N. *From Air Pollution to Climate Change. Atmospheric Chemistry and Physics*, 2nd ed.; John Wiley & Sons: New York, NY, USA, 2006.
12. Li, A.; Xie, P.H.; Liu, W.Q. Monitoring of Total Emission Volume from Pollution Sources Based on Passive Differential Optical Absorption Spectroscopy. *Acta Opt. Sin.* **2007**, *27*, 1537–1542. (In Chinese)
13. Wu, F.C.; Xie, P.H.; Li, A.; Chan, K.L.; Hartl, A.; Wang, Y.; Si, F.Q.; Zeng, Y.; Qin, M.; Xu, J.; et al. Observations of SO_2 and NO_2 by mobile DOAS in the Guangzhou eastern area during the Asian Games 2010. *Atmos. Meas. Tech.* **2013**, *6*, 2277–2292. [CrossRef]
14. Constantin, D.-E.; Merlaud, A.; van Roozendael, M.; Voiculescu, M.; Fayt, C.; Hendrick, F.; Pinardi, G.; Georgescu, L. Measurements of Tropospheric NO_2 in Romania Using a Zenith-Sky Mobile DOAS System and Comparisons with Satellite Observations. *Sensors* **2013**, *13*, 3922–3940. [CrossRef] [PubMed]
15. Xu, J.; Xie, P.-H.; Si, F.-Q.; Li, A.; Wu, F.-C.; Wang, Y.; Liu, J.-G.; Liu, W.Q.; Hartl, A.; Lok, C.K. Observation of tropospheric NO_2 by airborne multi-axis differential optical absorption spectroscopy in the Pearl River Delta region, south China. *Chin. Phys. B* **2014**, *23*, 9094210.
16. Wang, T.; Hendrick, F.; Wang, P.; Tang, G.; Clémer, K.; Yu, H.; Fayt, C.; Hermans, C.; Gielen, C.; Müller, J.F.; et al. Evaluation of tropospheric SO_2 retrieved from MAX-DOAS measurements in Xianghe, China. *Atmos. Chem. Phys.* **2014**, *14*, 11149–11164. [CrossRef]
17. Strong, K.; Bailak, G.; Barton, D.; Bassford, M.; Blatherwick, R.; Brown, S.; Chartrand, D.; Davies, J.; Fogal, P.; Forsberg, E.; et al. Mantra—A balloon mission to study the odd-nitrogen budget of the stratosphere. *Atmos. Ocean* **2005**, *43*, 283–299. [CrossRef]

18. Merlaud, A.; van Roozendael, M.; van Gent, J.; Fayt, C.; Maes, J.; Toledo-Fuentes, X.; Ronveaux, O.; de Mazière, M. DOAS measurements of NO_2 from an ultralight aircraft during the Earth Challenge expedition. *Atmos. Meas. Tech.* **2012**, *5*, 2057–2068. [CrossRef]
19. Schreier, S.F.; Peters, E.; Richter, A.; Lampel, J.; Wittrock, F.; Burrows, J.P. Ship-based MAX-DOAS measurements of tropospheric NO_2 and SO_2 in the South China and Sulu Sea. *Atmos. Environ.* **2015**, *102*, 331–343. [CrossRef]
20. Platt, U.; Stutz, J. *Differential Optical Absorption Spectroscopy: Principles and Applications*; Springer: Heidelberg, Germany, 2008.
21. Honninger, G.; von Friedeburg, C.; Platt, U. Multi axis differential optical absorption spectroscopy (MAX-DOAS). *Atmos. Chem. Phys.* **2004**, *4*, 231–254. [CrossRef]
22. Lin, J.T.; McElroy, M.B.; Boersma, K.F. Constraint of anthropogenic NOx emissions in China from different sectors: A new methodology using multiple satellite retrievals. *Atmos. Chem. Phys.* **2010**, *10*, 63–78. [CrossRef]
23. Bogumil, K.; Orphal, J.; Homann, T.; Voigt, S.; Spietz, P.; Fleischmann, O.C.; Vogel, A.; Hartmann, M.; Kromminga, H.; Bovensmann, H.; et al. Measurements of molecular absorption spectra with the SCIAMACHY preflight model: Instrument characterization and reference data for atmospheric remote-sensing in the 230–2380 nm region. *J. Photoch. Photobiol. A* **2003**, *157*, 167–184. [CrossRef]
24. Kraus, S. DOASIS. A Framework Design for DOAS. Ph.D. Thesis, University of Mannheim, Shaker Verlag, Heidelberg, Germany, 2006.
25. Kurucz, R.L.; Furenlid, I.; Brault, J.; Testerman, L. *Solar Flux Atlas from 296 nm to 1300 nm, National Solar Observatory Atlas No. 1*; Office of University Publisher, Harvard University: Cambridge, MA, USA, 1984.
26. Van Roozendael, C.F. *WinDOAS 2.1 Software User Manual*; IASB/BIRA: Brussel, Belgium, 2001.
27. Tim, D.; Steffen, B.; Udo, F.; Michael, G.; Christoph, K.; Lena, K.; Ulrich, P.; Cristina, P.-R.; Janis, P.; Thomas, W.; et al. The Monte Carlo atmospheric radiative transfer model McArtim: Introduction and validation of Jacobians and 3D features. *J. Quant. Spectrosc. Radiat. Transf.* **2011**, *112*, 1119–1137.
28. Yang, J.; Li, A.; Xie, P.; Liu, W.; Wu, F.; Wang, Y.; Zeng, Y. The Application of MM5 Wind Data in Monitoring of Regional Pollution based on Passive DOAS under different Atmospheric Stability Conditions in China. In Proceedings of the 2nd International Conference on Remote Sensing, Environment and Transportation Engineering, Nanjing, China, 1–3 January 2012; Volume 5.
29. Sun, N. The Research of Atmospheric Stability and Hoist Height in Zhenjiang. Master's Thesis, Jiangsu University, Zhenjiang, China, 2007. (In Chinese)
30. Pasquill, F.; Smith, F.B. *Atmospheric Diffusion*, 2nd ed.; Ellis Horwood Limited: London, UK, 1983.
31. Sutherland, R.A.; Hansen, F.V.; Bach, W.D. A quantitative method for estimating Pasquill stability class from windspeed and sensible heat flux density. *Bound. Layer Meteorol.* **1986**, *37*, 357–369. [CrossRef]